Chemical Engineering & Processing: Process Intensification 208 (2025) 110083

Contents lists available at ScienceDirect

Chemical Engineering and Processing - Process Intensification

journal homepage: www.elsevier.com/locate/cep

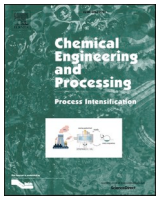

Structural optimization of separation layer and porous PES substrate for enhanced pervaporation desalination performance

Thi Thi Mar [a], Da Yin [b], Ziyu Fang [b], Tao Wang [b], Xi Dai [b], Bing Cao [b,*], Rui Zhang [b,c,*]

[a] College of Materials Science and Engineering, Beijing University of Chemical Technology, Beijing, 100029, PR China
[b] Engineering and Technology Research Center of Membrane for Chemical Industry, College of Chemical Engineering, Beijing University of Chemical Technology, Beijing, 100029, PR China
[c] Changzhou Key Laboratory of Biomass Green, Safe & High Value Utilization, Changzhou University, Changzhou 213164, PR China

ARTICLE INFO

Keywords:
Pervaporation
Desalination
Composite membrane
Polyethersulfone

ABSTRACT

Pervaporation membranes with water-selective properties hold great potential for desalination and brine concentration applications. In this study, a modified PES porous membrane with smaller pore sizes and enhanced interfacial support was used as the substrate. Ultrathin selective layers were fabricated on its surface via atomized spray coating, resulting in high-performance pervaporation membranes for desalination analysis. The study compares the effects of PVA and PEI on membrane performance under different crosslinking systems. At 82 °C, using a 3.5 wt.% sodium chloride solution, the PES composite membrane with a PEI/SPTA selective layer achieved a maximum flux of 180.35 ± 13.8 kg m^{-2} h^{-1}, with a salt rejection rate of 99.97% ± 0.2. Even at a higher brine concentration of 20 wt.%, the membrane maintained a flux of 49.77 ± 7.3 kg m^{-2} h^{-1} at 72 °C. The membrane's high salt rejection and stable performance under complex operating conditions demonstrate that pervaporation composite membranes prepared with low-surface-porosity substrates offer enhanced cycle stability and industrial potential in real-world desalination and concentration applications.

1. Introduction

Freshwater scarcity is the third most pressing global crisis, after food and oil shortages, posing a significant threat to human life and hindering social progress [1]. Desalination of brackish water has emerged as a critical technology for supplying fresh water in regions experiencing water scarcity. This process involves removing salts and minerals from seawater or brackish water to make it suitable for consumption [2]. The most common types of desalination technologies are thermal processes and membrane-based processes, which are used to produce fresh water and solve water shortages [3]. Membrane technology provides exceptional operational stability, high productivity, and low chemical costs, making it widely adopted in environmental applications for water treatment [4–7]. The treatment of high-salinity wastewater has gained increasing attention in recent years [8,9]. Pervaporation (PV) membrane separation has shown particular advantages in the desalination and concentration of complex aqueous solutions [10]. This advantage arises from the dense, selective separation layer of PV composite membranes, where water is transported through a solution-diffusion mechanism driven by a transmembrane vapor pressure difference. Unlike conventional processes, the diffusion rate is only minimally affected by ion concentration, and the selective layer effectively prevents the diffusion of volatile organics and other undesirable components into the permeate. PV is particularly effective for desalinating high-salinity solutions [11,12].

To achieve high water flux, a hydrophilic, dense separation layer is often fabricated atop a porous support layer with low mass transfer resistance [13,14]. Water molecules dissolve into the membrane's surface, diffuse through the separation layer, and exit from the lower surface. This diffusion process is influenced by the nature and thickness of the separation layer, as the efficiency of molecular transport is directly impacted by the thickness of the membrane, making it a key factor in overall performance [2,15]. To ensure the stability and efficiency of the separation layer, porous support layers are commonly made from commercial microfiltration and ultrafiltration membranes using materials such as polypropylene, polysulfone, polyvinylidene fluoride (PVDF), and polyethersulfone (PES) [16–18]. Among these materials, porous PES membranes are favored in water treatment and pervaporation processes because of their ease of fabrication, outstanding mechanical properties, and superior chemical and thermal stability [19,

* Corresponding authors.
E-mail addresses: bcao@mail.buct.edu.cn (B. Cao), zhangrui1@mail.buct.edu.cn (R. Zhang).

https://doi.org/10.1016/j.cep.2024.110083
Received 16 October 2024; Received in revised form 11 November 2024; Accepted 20 November 2024
Available online 24 November 2024
0255-2701/© 2024 Elsevier B.V. All rights are reserved, including those for text and data mining, AI training, and similar technologies.

20]. Additionally, for optimal performance in PV applications, the support layer must provide strong mechanical support to the ultrathin separation layer while maintaining smooth surface characteristics, adjustable mass transfer resistance, and stable interfacial bonding, making PES an ideal choice for use as the substrate in high-performance PV desalination membranes. However, the inherent hydrophobicity and low surface porosity of PES present challenges in establishing strong interfacial bonding with the selective layer and minimizing mass transfer resistance, both of which are essential for efficient PV desalination [21]. To overcome these challenges, hydrophilic polymer additives like polyvinylpyrrolidone (PVP) are commonly incorporated to increase the hydrophilicity of the PES substrate [14]. In addition to improving hydrophilicity, these additives can modify the casting solution properties during phase inversion, resulting in an improved pore structure and, consequently, better separation performance [16,22,23,24]. However, the stability of water-soluble polymers used as pore-forming agents in the substrate layer tends to fluctuate during the separation process due to migration and other structural changes. These alterations in the pore structure can significantly affect the long-term stability and performance of PV composite membranes.

Furthermore, in the fabrication of the separation layer in pervaporation (PV) desalination composite membranes, polyethyleneimine (PEI) and polyvinyl alcohol (PVA) have become essential materials for separation layer structure and design due to their hydrophilicity and film-forming capabilities. Their hydrophilic properties, however, differ under conditions of saturated water absorption due to their unique chemical structures and functional groups. PEI is a polymer consisting of ethyleneimine units and densely distributed amine groups along both its main and side chains, which include primary, secondary, and tertiary amines. These highly polar amine groups not only facilitate crosslinking reactions but also form multiple hydrogen bonds with water molecules, imparting PEI with remarkable hydrophilicity. In contrast, PVA is composed of vinyl alcohol units with side-chain hydroxyl groups arranged in a more ordered, crystalline structure. While hydroxyl groups also serve as reactive functional groups forming hydrogen bonds with water, they are positioned on side chains attached to a hydrophobic hydrocarbon backbone, which allows for stable swelling systems during crosslinking. Thus, a comparative analysis and optimization of these two hydrophilic polymers under different crosslinking systems is required to enhance water transport properties within the PV desalination membrane's separation layer structure.

Building upon the prior analysis, this study employs the non-solvent induced phase separation (NIPS) method to fabricate a porous polyethersulfone (PES) substrate with refined pore uniformity and enhanced support stability. For the first time, an ultrathin selective layer was applied on the PES surface via spray-coating to develop a composite membrane for pervaporation (PV) desalination. Building on previous research in which polyvinyl alcohol (PVA) was used as the selective layer in PV membranes, this work introduces polyethyleneimine (PEI), a polymer with superior hydrophilicity, for comparison [25,26]. The study evaluates the hydrophilic stability and desalination performance of the membrane under various crosslinking systems, following polymer crosslinking with the PES substrate. Thermally-induced crosslinked polymer networks were applied on the PES surface to stabilize the selective layer. Critical parameters such as pure water flux, desalination efficiency, and antifouling properties of both the PES substrate and the PV composite membranes were evaluated. The goal of this research is to enhance the stability of the substrate support while optimizing the materials in the selective layer to improve mass transfer rates and overall membrane performance. These findings provide valuable insights for advancing the practical application of pervaporation desalination technology.

2. Experimental

2.1. Materials

Polyethersulfone (PES, Udel P1700) was purchased from Solvay Co., Ltd. Polyvinylpyrrolidone (PVP K-30) was bought from Gobekie Co., Ltd. N-methyl-2-pyrrolidone (NMP, purity > 99 %), n-hexane (purity > 99 %), methanol (purity > 99 %), and concentrated sulfuric acid (H_2SO_4, purity: 98 %) were provided by Tianjin Damo Chemical Reagent Factory (China). Polyethylene terephthalate (PET) non-woven was obtained from Shanghai Poly Technology Co., Ltd. Deionized water (DI) was produced using a laboratory-equipped water purification system (Smart-Q 15). Sodium chloride (NaCl, purity: 99.9 %), ammonium chloride (NH_4Cl, purity: 99.95 %), lithium chloride (LiCl, purity: 95.0 %), Tween-20, and sodium dodecyl benzene sulfonate (SDBS, purity > 98 %) were purchased from Sinopharm Chemical Reagent Co., Ltd. (China). 4-sulfophthalic acid (SPTA), poly acrylic acid co-2-acrylamido-2-methyl propane sulfonic acid (P(AA-AMPS), M_w: 2000–5000 g mol^{-1}), and ethyleneimine polymer (PEI, purity ≥ 99 %, M_w: 600 g mol^{-1}) was purchased from Shandong Usolf Chemical Technology Co., Ltd. Poly (vinyl alcohol) (PVA, hydrolysis degree: 99.4 %, M_w: 105,000 g mol^{-1}) was bought from Gobekie Co., Ltd. All chemicals except NMP were used as received. NMP was dried using the 4 Å molecular sieves before use.

2.2. Fabrication of substrate membrane

Based on the non-solvent-induced phase separation technology, PES substrate membranes were prepared, as shown in Fig. 1. In particular, a 14:4:1:81 wt ratio polymer coating solution containing PES, PVP, LiCl, and NMP was prepared. Subsequently, the dope solution was swiftly coated onto a smooth PET non-woven fabric using a 200 μm slit blade at room temperature. Gelatinous polymer membranes containing PET substrates are phase-converted by using deionized water. After 95 h of immersion in deionized water to eliminate all traces of solvent and soluble substances, the membranes were re-soaked in methanol for 30 min and n-hexane for 30 min, respectively. Eventually, the PES membrane is removed and allowed to air dry at room temperature.

2.3. Preparation of composite membrane

To create a homogeneous solution, polyvinyl alcohol and polyethyleneimine polymer solutions are initially prepared using deionized water and various crosslinkers. Subsequently, air bubbles are removed from the solutions using an ultrasonic bath. Table 1 presents the mass concentrations of PEI and PVA polymer solutions used for preparing the selective layer, along with the mass percentage compositions of crosslinking agents SPTA and P(AA-AMPS) in the corresponding systems.

An airbrush is then employed to apply the polymer solution onto the surface of the PES substrate layer. The specific operating parameters of the airbrush are detailed as follows: the distance between the airbrush and the membrane is maintained at 15 cm, with the airbrush operating at a pressure of 2–3 bar. After coating, the resulting membrane is crosslinked in an oven at 100 °C for 20 min following the evaporation of the solvent. This process results in the formation of the composite membrane, as illustrated in Fig. 2. In addition, Table 2 presents the fabricated composite membranes made with different crosslinkers.

2.4. Characterization methods

The prepared membranes were characterized by several techniques and instruments. Fourier transform infrared spectroscopy (ATR-FTIR, Nicolet 560) was used to investigate the chemical structures of the membranes with different crosslinkers. The surface and cross-section morphologies of the membranes were performed with the scanning electron microscope (SEM, JSM-7800F, JEOL Ltd., Japan). The surface roughness was performed with the atomic force microscope (AFM,

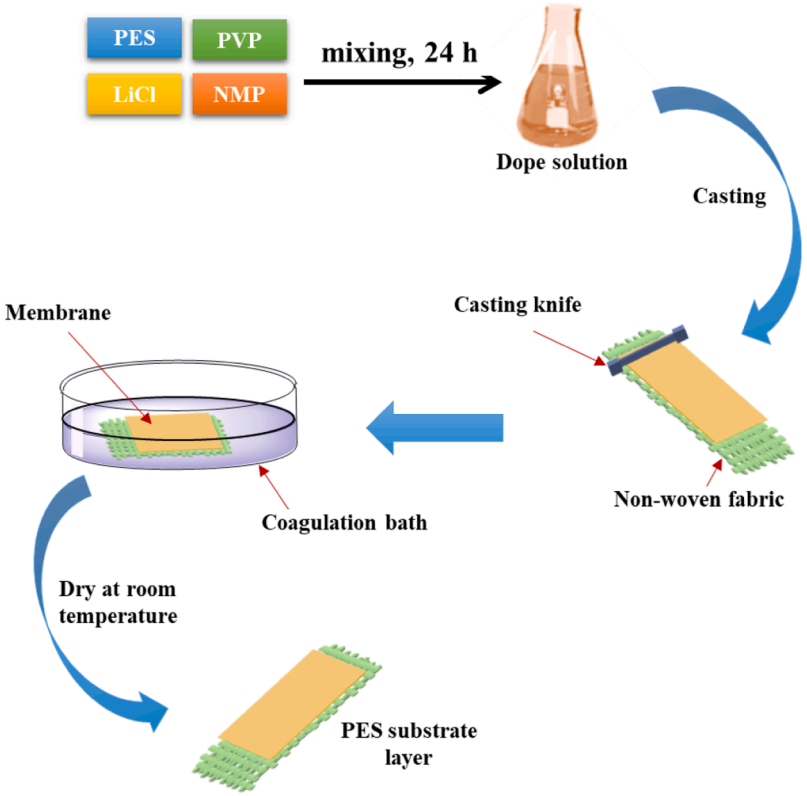

Fig. 1. A schematic diagram process for the preparation of the PES substrate layer.

Table 1
Composition of solution for the coating layer.

PEI	PVA	SPTA	P(AA-AMPS)
1 wt.%	1.5 wt.%	0.1 wt.%	0.3 wt.%

Dimension Fastscantm, Bruker, USA). The water contact angle of the membranes was tested using the contact angle Goniometer device at least five times, and the value was reported.

2.5. Water uptake of the membranes

The membrane was dried in a vacuum oven at 100 °C for 30 min. After drying, the membrane was weighed and then immersed in solutions with various conditions for at least 12 h, including different pH values (1, 7, and 14), salt concentrations (3.5 wt.%, 7 wt.%, and 10 wt. %), and temperature (2 °C, 30 °C, and 60 °C), to achieve absorption equilibrium. Before determining the wet weight (W_s), gently clean the membrane surface with filter paper to remove excess water. Then, determine the dry weight (W_d). The water absorbency (WA) is calculated

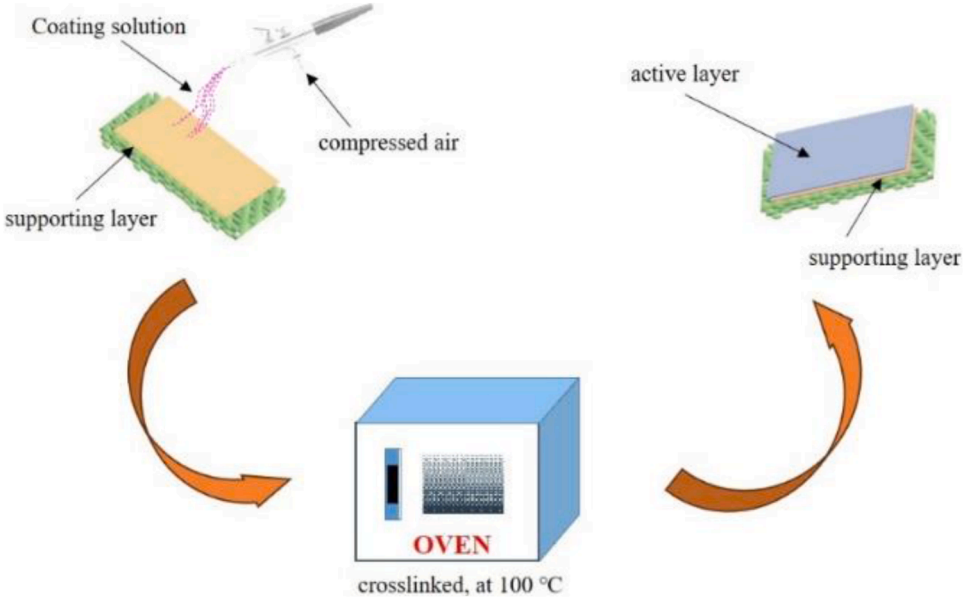

Fig. 2. Process flow diagram for the PES composite membrane preparation.

Table 2
List of composite membranes fabricated with different crosslinkers.

Membrane ID	Substrate	Coating Layer	Crosslinkers
PES/PVA/P(AA-AMPS)	PES	PVA/P(AA-AMPS)	P(AA-AMPS)
PES/PVA/SPTA	PES	PVA/SPTA	SPTA
PES/PEI/P(AA-AMPS)	PES	PEI/P(AA-AMPS)	P(AA-AMPS)
PES/PEI/SPTA	PES	PEI/SPTA	SPTA

using Eq. (1):

$$WA = \frac{W_s - W_d}{W_d} \times 100\% \quad (1)$$

2.6. Permeability of PES substrate layer

The pure water flux of the membrane was measured using a home-made dead-end ultrafiltration device, as shown in Supplementary Figure 1. The membrane's area was 1.26 cm^2. Initially, the membrane was pressurized at 0.5 MPa for 30 min, and then the pressure was reduced to 0.1 MPa. The pure water flux of the PES supporting membrane at room temperature is calculated using Eq. (2).

$$J = \frac{M}{A_1 \times t_1} \quad (2)$$

where J was water flux (kg m^{-2} h^{-1}), M was the weight of permeate (kg), A_1 was the effective membrane area (m^2), and t_1 was operation time (h).

The gas transport resistance of the PES membrane was measured using a laboratory-manufactured gas permeation cell, as shown in Supplementary Figure 2. At high transmembrane pressures, gas permeation cells typically measure a range of N_2 fluxes. Gas permeability provides information about the average pore size and porosity of the PES substrate layer. The relationship between gas flux and transmembrane pressure can then be confirmed by applying Eq. (3).

$$Q = \frac{V}{A \times t} \quad (3)$$

where Q was the gas flux of N_2 (L m^{-2} h^{-1}), V was the volume of the permeated gas (L), A was the effective membrane area (m^2), and t was the permeation time (h).

2.7. Evaluation of PV performance test

The pervaporation performance of composite membranes was tested using bespoke equipment. In this work, the separation capacity of the membrane was evaluated using monovalent salts such as NaCl, NH_4Cl, and LiCl. Briefly, after the composite membrane is placed in a membrane cell and the feed solution is transferred through the membrane at a steady temperature, liquid nitrogen is used to condense the permeate components in a cold trap. A vacuum pump maintains the permeate side pressure, utilizing an effective membrane area of 3.14×10^{-3} m^2. Eq. (4) is then applied to calculate the pervaporation flux value (J).

$$J = \frac{M}{s_1 \times t_1} \quad (4)$$

where M was the weight of the permeated liquid collected in the cold trap (kg), s_1 was the effective membrane area (m^2), and t_1 was the operation time (h). Eq. (5) is used to measure the rate of salt rejection (R_{NaCl}, %).

$$R_{NaCl} = \frac{C_{feed} - C_{permeate}}{C_{feed}} \times 100\% \quad (5)$$

where C_{feed} and $C_{permeate}$ were the ionic concentrations of the feed and permeate solutions expressed in m. S. cm^{-1}.

3. Results and discussion

3.1. Surface chemical structure analysis

The selective coating layers were prepared by assessing the base systems of PVA and PEI separation layers using two different crosslinking agents: SPTA and P(AA-AMPS). The Fourier Transform Infrared (FTIR) spectra are shown in Fig. 3(a), while Fig. 3(b) illustrates a schematic representation of the reactions between the PVA and PEI polymers with crosslinking agents SPTA and P(AA-AMPS).

In the PVA-coated solution membrane, the absorption peaks between 3300 cm^{-1} and 3400 cm^{-1} are attributed to the stretching vibration of the -OH groups in PVA, while the strong absorption band around 1100 cm^{-1} is due to symmetric C—O stretching vibrations [3,27,28]. In the P(AA-AMPS) system, the C—N stretching frequency of the aliphatic amide in the crosslinking agent is prominently observed in the range of 1100 cm^{-1} to 1150 cm^{-1}. Additionally, the stretching vibration of C = O occurs near 1700 cm^{-1}, and the stretching frequency of CH_2 is around 2900 cm^{-1} [29].

The FTIR spectrum of a PEI solution without a crosslinker exhibits several characteristic peaks. A broad peak around 3300 cm^{-1} indicates the presence of primary and secondary amine groups, attributed to N—H stretching. The peak at 2949 cm^{-1} corresponds to the aliphatic C—H bonds, while peaks in the 1429 cm^{-1} range are related to N—H bending vibrations. Additionally, peaks at 1080 cm^{-1} are indicative of C—N stretching, confirming the presence of amine functionalities and the aliphatic structure of PEI [30,31]. When PEI is crosslinked with SPTA, the FTIR spectrum shows distinct changes. New strong peaks in the 1000 −1250 cm^{-1} region indicate the presence of sulfonate groups from the crosslinker. Peaks around 1500 −1600 cm^{-1} correspond to the carboxylic acid groups of the crosslinkers. The N—H stretching region (3300 −3500 cm^{-1}) may exhibit broadening, indicating amide bonding and hydrogen bonding interactions between the amine groups of the PEI and the sulfonic or carboxylic acid groups of the crosslinkers. The appearance of new peaks around 1600 cm^{-1} could suggest the formation of amide bonds, underscoring the covalent interactions resulting from the cross-linking process. In conclusion, the comparison of FTIR spectra for PEI, both with and without the SPTA crosslinker, reveals significant changes that indicate successful crosslinking. The appearance of new peaks, shifts in existing peaks, and changes in peak intensities provide valuable insights into the chemical interactions and structural modifications induced by the crosslinking process.

3.2. Morphology and structure of membranes

The PES substrate layer has a uniform surface with numerous evenly distributed pores, as shown in Fig. 4(a_1). Fig. 4(b_1, c_1, d_1, and e_1) illustrates the membrane structure after applying the PVA and PEI coating solutions. SEM results confirm that a uniform, defect-free, and low-roughness PEI/PVA coating was formed on the surface of the PES membrane. The surface of the PES composite membrane appears very flat and smooth, indicating the formation of a dense, defect-free structure. Fig. 4(a_2, b_2, c_2, d_2, & e_2) displays the cross-sectional view of the composite membranes and the asymmetric PES substrate layer. The substrate layer shows an increase in finger-like voids with open structures. This can be attributed to two factors: (i) the rapid precipitation of the casting solution, leading to the formation of finger-like structures on the non-woven paper, and (ii) the swift exchange of solvents and non-solvents during phase separation, which contributes to the development of this structure [32]. Additionally, different coating solutions with various crosslinkers are applied to the PES membrane. All composite membranes demonstrate the presence of a thin top skin layer supported by a finger-like sublayer.

Fig. 5 presents AFM images of the PES substrate layer and the PES/PEI/SPTA composite membrane. Additionally, Table 3 provides surface roughness data for these samples, including mean roughness (R_a),

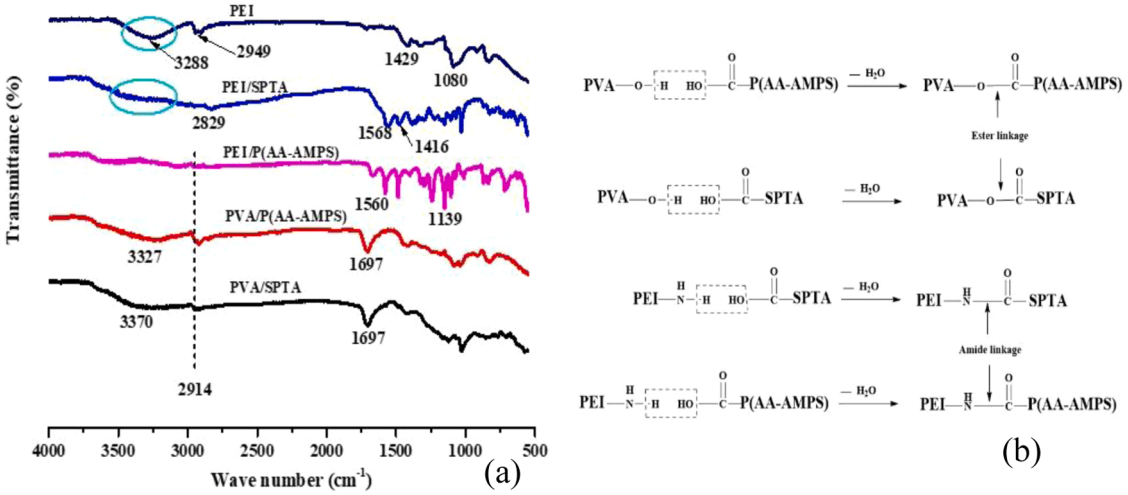

Fig. 3. FTIR spectrum (a) and reactions (b) of active layers with crosslinkers SPTA and P(AA-AMPS).

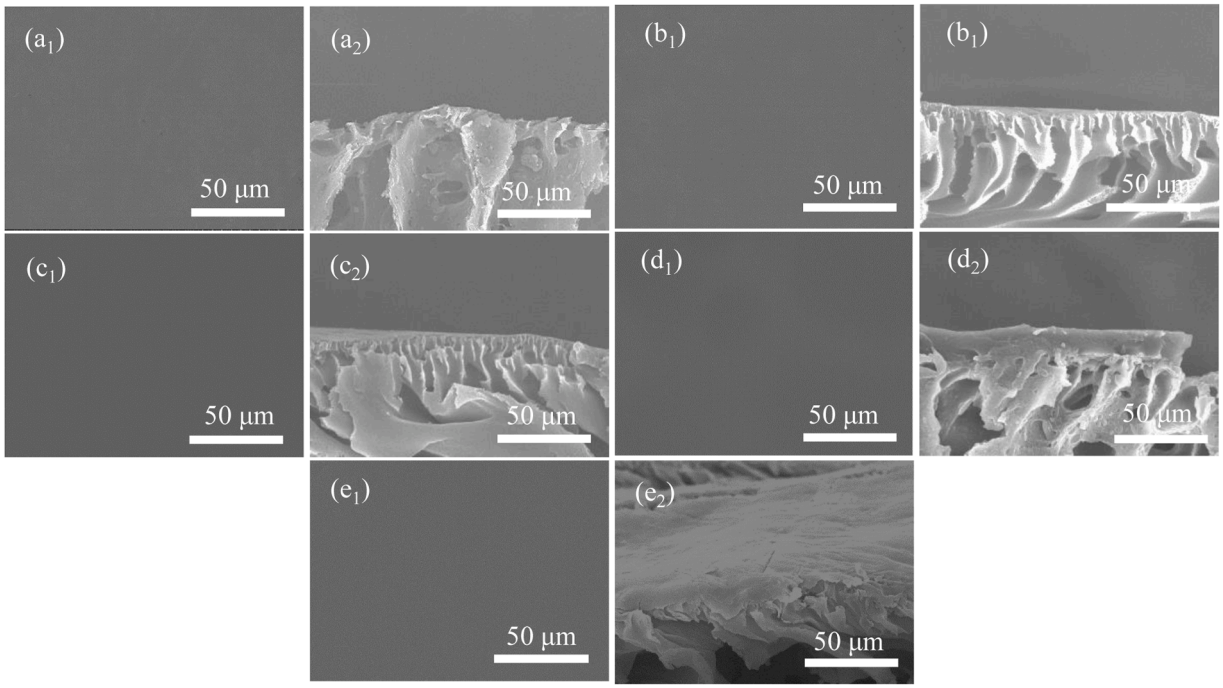

Fig. 4. Surface morphology and cross-section SEM images of the PES substrate layer (a_1, a_2) and PES composite membranes with PEI/SPTA (b_1, b_2), PEI/P(AA-AMPS) (c_1, c_2), PVA/SPTA (d_1, d_2), and PVA/P(AA-AMPS) (e_1, e_2) coating solutions.

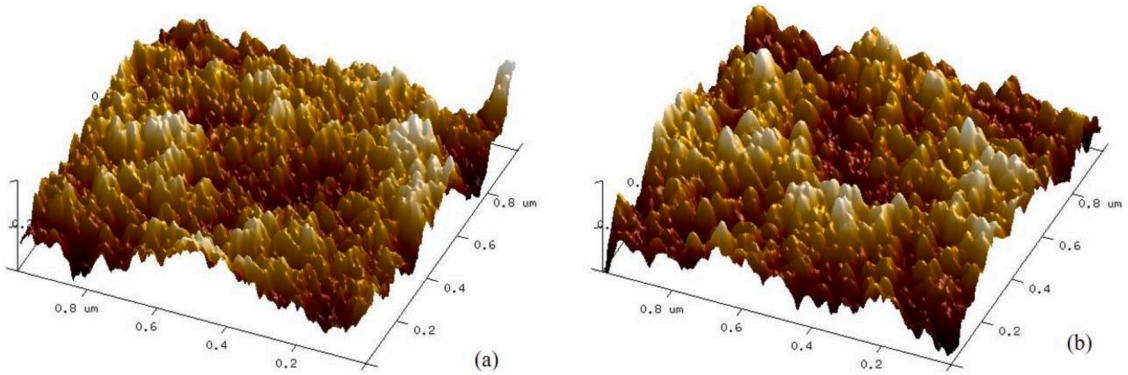

Fig. 5. Three dimensions AFM images of (a) PES substrate layer at room temperature and (b) PES/PEI/SPTA composite membrane at 100 °C.

maximum roughness depth (R_{max}), and root mean square (R_q). The composite membrane exhibits lower roughness values compared to the conventional PES substrate layer. This observed smoothness of the PES/PEI/SPTA composite membrane, as opposed to the rougher PES substrate layer, can be attributed to several factors, including material properties, the coating process, and the effect of crosslinking. Polyethyleneimine is known for forming uniform, smooth films when applied to surfaces, while SPTA serves as an effective crosslinker that enhances the structural integrity and smoothness of the PEI layer. The molecular interactions between PEI and SPTA result in a more homogeneous distribution of polymer chains, leading to a smoother surface. The spray coating process ensures that the PEI/SPTA solution spreads uniformly across the PES substrate, filling in surface irregularities and creating a smooth overlay [33,34]. The cross-linking effect of SPTA further contributes to surface smoothness by densifying the film, reducing the mobility of polymer chains, and minimizing surface asperities. Atomic force microscopy topographical data supports this explanation, showing lower roughness parameters for the PEI/SPTA composite membrane compared to the PES layer. AFM images reveal fewer and smaller surface features on the composite membrane, indicating a more homogeneous and continuous surface. Overall, the smoother surface of the PEI/SPTA composite membrane is attributed to the effective masking of the underlying PES roughness by the coating and crosslinking processes, which are crucial for applications requiring enhanced surface smoothness and mechanical stability.

3.3. Performance analysis of PES substrate

The pervaporation performance of the composite membrane is influenced not only by the hydrophilicity of the separation layer but also significantly by the gas permeation efficiency of the porous support substrate. To effectively control the porous substrate layer and provide a suitable transition for the separation structure, it is essential to assess and optimize its gas permeation efficiency. Optimizing the PES substrate layer involved systematically adjusting key parameters in the membrane fabrication process to achieve the desired balance between mechanical strength, porosity, and gas permeability. Initially, the polymer concentration in the casting solution was varied to control the thickness and pore structure of the substrate layer. Increasing the concentration of PES reduced overall porosity, resulting in a more robust substrate layer, but it also increased the membrane's thickness, which negatively impacted gas permeability. In addition, incorporating a small amount of polyvinylpyrrolidone (PVP) as a pore-forming agent enhanced pore connectivity, further improving the gas permeability of the substrate layer without compromising its mechanical stability. Table 4 presents the contact angle, pure water flux, and gas permeability of the PES substrate layer.

The optimized PES substrate membrane, with a water contact angle of only 51.18° ± 3.2, demonstrated excellent hydrophilic properties, ensuring good integration with the separation layer and maintaining stability. Thickness and pore structure are major factors affecting gas permeability, with a noticeable decrease in gas permeability as membrane thickness increases. The overall pore size and structure of the substrate membrane play a crucial role in forming unobstructed gas channels, which represent one of the key constraints on the performance of the substrate layer [35]. After optimizing the PES substrate layer's structure, we conducted separate tests on the pure water permeability and gas permeability of the support membrane under standard conditions. Nitrogen was used as a substitute for water vapor to assess gas permeability. The water flux was measured at 12.838 ± 1.1 kg m^{-2} h^{-1}, while nitrogen permeability was 2925.05 ± 27.8 L m^{-2} h^{-1}. The experimental data clearly show that the gas transmission capacity of the support layer is approximately 230 times greater than that of the liquid. Therefore, it can be inferred that the transport resistance of the substrate layer in the composite membrane does not significantly impede overall permeability.

Table 3
Surface roughness of the PES supporting layer and composite layer.

Membrane ID	Temperature (°C)	R_a (nm)	R_q (nm)	R_{max} (nm)
PES supporting layer	Room temperature	36.8 ± 4.1	47.1 ± 7.1	420 ± 31.2
PES/PEI/SPTA composite membrane	100 °C	3.62 ± 0.4	4.62 ± 0.5	32.2 ± 2.1

Table 4
Contact angle, gas permeability, and water vapor flux of the PES supporting layer.

Membrane ID	WCA (.)	J (kg m^{-2} h^{-1})	Q (L m^{-2} h^{-1})
PES supporting layer	51.18 ± 3.2	12.838 ± 1.1	2925.05 ± 27.8

3.4. Hydrophilicity impact on membranes

The water contact angle of the composite membrane and the substrate layer was measured using a contact angle measuring instrument, with the resulting values displayed in Fig. 6. The experimental results demonstrate that the addition of PVP significantly enhances the hydrophilicity of the PES substrate. Both PEI and PVA coating layers further increase the hydrophilicity of the PES membrane under different crosslinking systems, primarily due to the presence of more hydrophilic groups in the separation layer system [36]. The PEI coating solution containing SPTA crosslinker demonstrates superior surface wettability and affinity compared to PVA, attributed to the highly polar amine groups and hydrogen bonding, which make PEI more hydrophilic. In the PEI separation layer with SPTA, the dense arrangement of amine groups and the introduction of sulfonic groups from SPTA provide additional sites for hydrogen bonding and interaction with water. The structural flexibility of the PEI-SPTA network further enhances the accessibility and interaction of hydrophilic groups with water molecules. In contrast, P(AA-AMPS), while hydrophilic, has fewer hydrophilic groups and lacks structural flexibility, resulting in relatively lower hydrophilicity. Thus, the extensive hydrogen bonding capability and strong ionic interactions in the SPTA system make it a more hydrophilic layer compared to P(AA-AMPS), theoretically improving the water dissolution and diffusion rate during the membrane separation process.

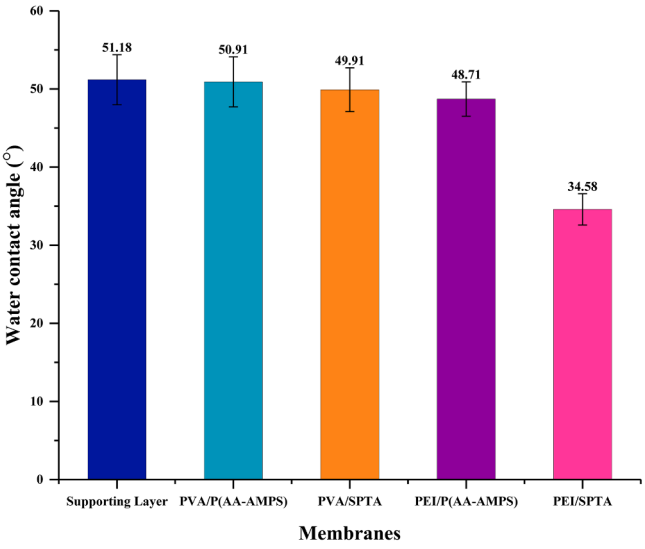

Fig. 6. Water contact angle of PES substrate layer and PES composite membranes.

In the presence of aqueous solutions, the water swelling process of PV composite membranes under varying conditions is crucial for evaluating desalination efficiency, as it represents a key characteristic in assessing the permeability of water molecules through the separation membrane. Various composite membrane systems based on the PES substrate layer structure were prepared. The water swelling behavior of the composite membranes was studied concerning pH, temperature, and concentration. The experiment revealed that both the substrate layer and composite membrane exhibited maximum water absorption at high temperatures, low salt concentrations, and low pH levels, as shown in Fig. 7.

In Fig. 7(a), the water absorption capacity of the composite membrane in sodium chloride solution decreases as the concentration increases. As the salt concentration rose at room temperature, the formation of hydrated ions from water molecules and ions led to the surrounding water molecules forming a layer which increased the overall structural volume. This, in turn, reduced the binding forces and diffusion capability between water molecules and the separation layer molecules. At higher salt concentrations, only independently diffusing water molecules could enter the three-dimensional polymer network matrix at a relatively faster rate, causing membrane swelling and a decrease in water absorption [37,38]. The impact of pH on membrane water absorption at various levels (pH 1, pH 7, and pH 14) is illustrated in Fig. 7(b), showing a similar effect to that observed with increasing salt ion concentration. By examining how the membrane absorbs water across different pH values, one can assess its chemical stability and whether it retains structural integrity and functionality in acidic or alkaline environments. This testing also ensures that the membrane maintains consistent water absorbency, regardless of pH fluctuations, which is crucial for applications where water pH may vary. Additionally, understanding the membrane's interactions with water molecules at different pH levels can guide future design optimizations and enhancements. Overall, this testing establishes the membrane's reliability and robustness for practical applications. Fig. 7(c) demonstrates how temperature influences the water absorption rate of the membrane. The membrane was placed in a refrigerator to maintain a temperature of 2 °C. At 2 °C, the swelling capacity of the membrane is minimal, as the movement of polymer chain segments and small molecules in the separation membrane is inhibited at low temperatures, resulting in a decrease in swelling performance. Conversely, at 60 °C, the movement of polymer chain segments is enhanced, and due to the increased diffusion of water molecules into the polymer network of the membrane, the amount of absorbed water is significantly higher, enhancing the saturation water absorption capacity.

3.5. Pervaporation performance of the composite membrane

On the surface of the PES substrate layer, PV composite membranes were prepared using different separation layer systems, and their effects on desalination performance were investigated. As shown in Fig. 8(a), PV tests were conducted at 72 °C using a 3.5 wt.% NaCl solution and the composite membranes with different cross-linking systems maintained high salt rejection rates. The PES composite membranes with P(AA-AMPS) crosslinker can form hydrogen bonds, but there are differences in the density and accessibility of these hydrophilic groups compared to the PEI-SPTA system. The PES composite membrane with PEI/SPTA coating layer exhibited higher flux than the other coating layers, likely due to better porosity, hydrophilicity, and stability in the PEI/SPTA combination. This difference in performance may be attributed to several factors. PEI, when used with SPTA, likely forms a more porous and less dense network, enhancing water permeability more effectively than PVA with SPTA. Additionally, the PEI/SPTA combination might improve the hydrophilicity of the membrane surface better than PVA/SPTA, reducing fouling and facilitating better water transport. Furthermore, the chemical interactions between PEI, SPTA, and the PES membrane could result in a more stable and uniform coating, contributing to the higher flux observed. Among all membranes, the PEI/SPTA composite membrane exhibited the highest flux value, which can be well explained by the water absorption data of the composite membrane at 72 °C. This system demonstrated higher water absorption efficiency and lower water contact angle at this condition. Furthermore, as shown in Fig. 8(b), with the temperature increasing from 42 °C to 82 °C, the permeation flux of the PES/PEI/SPTA composite membrane significantly increased at 82 °C, reaching 180.35 ± 13.8 kg m^{-2} h^{-1} at 82 °C. This increase was primarily due to the significant increase in the saturated vapor pressure difference between the upstream and downstream, enhancing the driving force for water molecules to permeate and vaporize [27]. Additionally, the enhanced mobility of the cross-linked segments of the separation layer with increasing temperature, combined with the increased driving force, significantly accelerated the diffusion rate of water molecules dissolved in the membrane [7]. However, due to the excellent swelling stability of the cross-linking system, the salt retention rate for desalination remained stable.

One of the major advantages of pervaporation desalination lies in its ability to handle high-concentration brine solutions. Here, we demonstrate that the PES/PEI/SPTA TFC membrane can effectively treat NaCl solutions with concentrations as high as 20 wt.%. As depicted in Fig. 8(c), at 72 °C, as the NaCl content increases from 3.5 wt.% to 20 wt.%, the water flux of the PES/PEI/SPTA composite membrane experiences a sharp decline, dropping from 141.55 ± 9.8 kg m^{-2} h^{-1} to 49.77 ± 7.3 kg m^{-2} h^{-1}. This decrease can be attributed to two factors. Firstly, the reduced water absorption of the separation layer with increasing salt concentration is influenced by the small molecule dissolution diffusion mechanism. Secondly, with the rise in feed solution salinity, the concentration polarization on the membrane surface intensifies, diminishing the driving force for water molecules to permeate through the membrane, consequently reducing the overall flux. Fig. 8(d) further compares and analyzes the PV desalination performance of the TFC

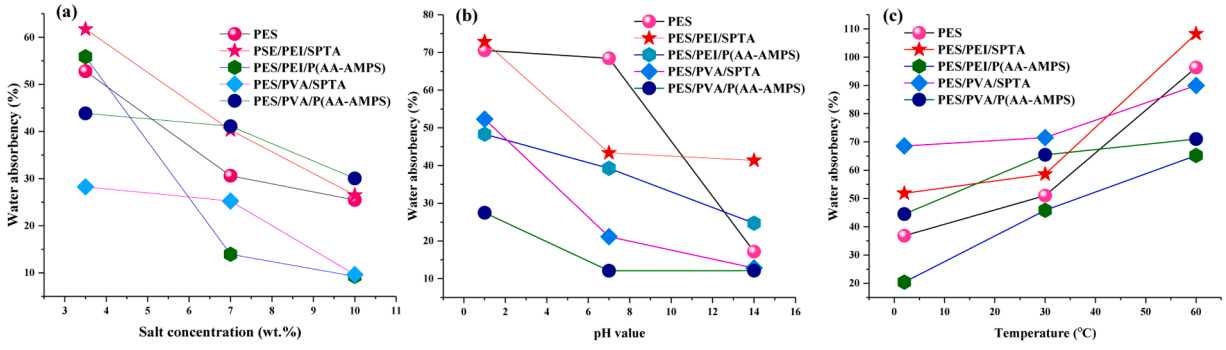

Fig. 7. Water absorbency of PES substrate layer and composite membranes with various parameters (a) salt concentration (NaCl, wt.%), (b) pH value, and (c) temperature (°C).

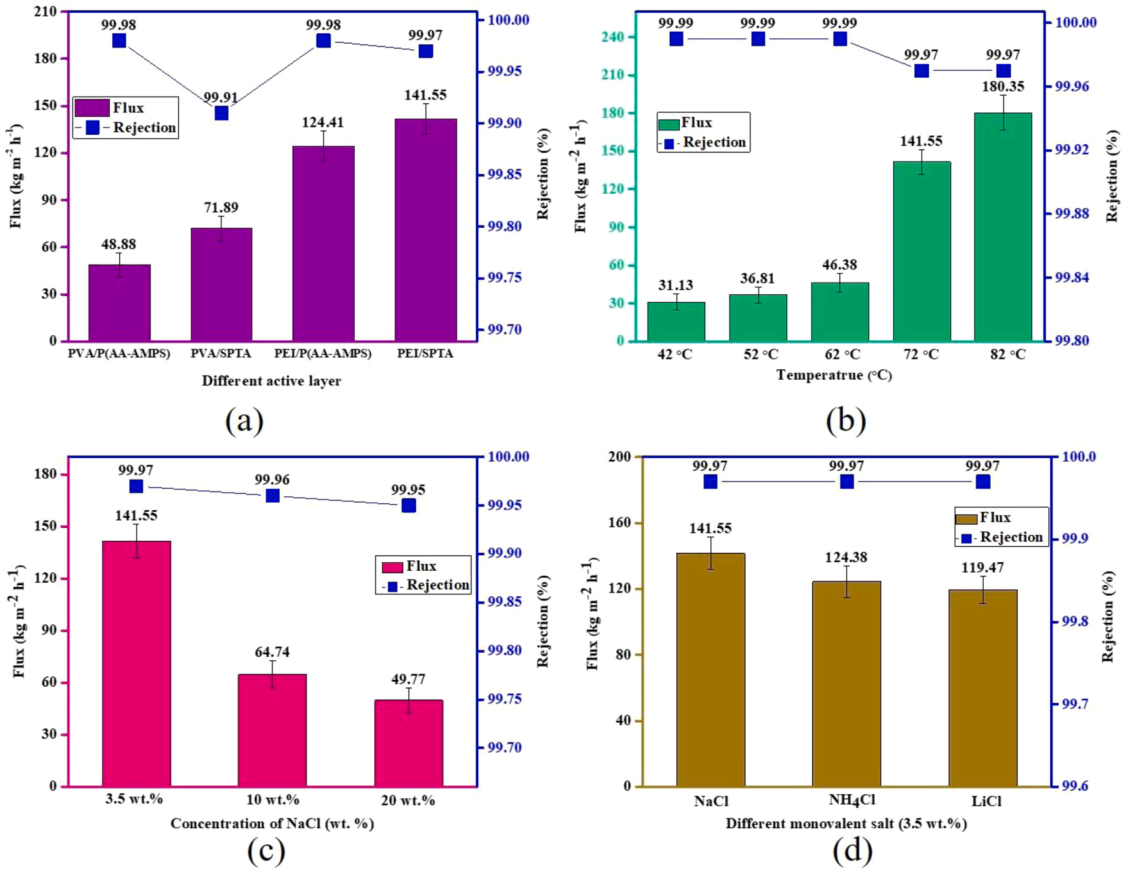

Fig. 8. Desalination performance of the PES composite membrane using various active layers at 72 °C (a), desalination performance of PES/PEI/SPTA composite membrane at feed temperatures ranging from 42 °C to 82 °C (b), feed solutions containing 3.5 wt.% to 20 wt.% NaCl at 72 °C (c), and various monovalent salts at 72 °C (d).

membrane under identical concentration conditions (3.5 wt.%) for various monovalent salts (e.g., NaCl, NH_4Cl, and LiCl) at 72 °C. The data indicate that the TFC membrane with the PEI/SPTA selection layer exhibits a retention rate of over 99.9 % for monovalent salts, albeit with slight variations in water flux for different ions, which can be attributed to the hydration of ions in solution and the membrane surface charge effect.

3.6. *Long-term desalination and anti-fouling property*

Permeation performance under complex liquid compositions is crucial for evaluating the stable operation of separation membranes. The

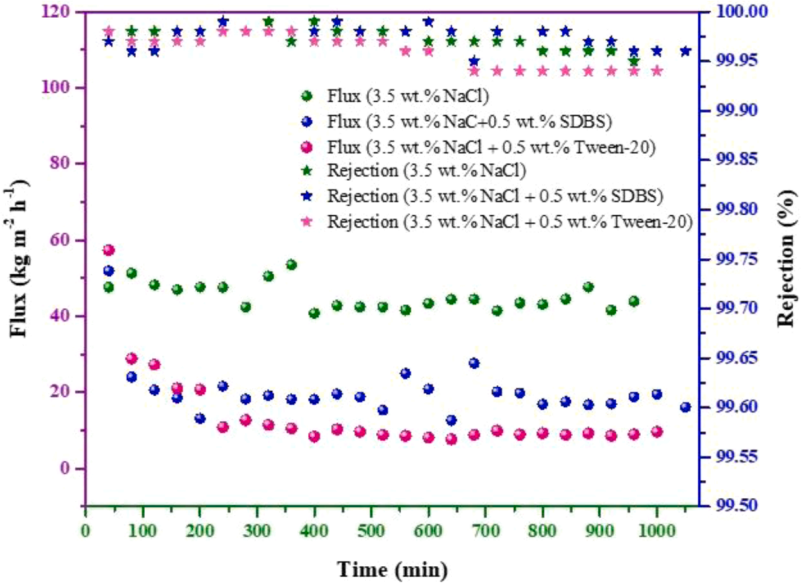

Fig. 9. Long-term desalination and antifouling performance of the PES/PEI/SPTA composite membrane (at 72 °C, 100 Pa).

PES/PEI/SPTA system, which showed superior performance in preliminary tests, was selected and subjected to stable cross-linking at 100 °C for 30 min. The resulting composite membranes were then tested for fouling resistance and continuous operational stability. As shown in Fig. 9, 3.5 wt.% NaCl solutions were used, with 0.5 wt.% anionic surfactant (SDBS) and 0.5 wt.% nonionic surfactant (Tween-20) added as model contaminants. Test results were collected every 20 min during long-term pervaporation testing. Over 980 min of operation, the separation membranes consistently maintained stable salt rejection performance, with permeation flux stabilizing after an initial decrease.

One of the main reasons for the reduction in flux is the polarization effect caused by organic contaminants on the membrane surface, as observed over extended operational periods [6,39]. Overall, the PV membranes in this system demonstrate excellent antifouling properties and stable operational performance. The comparison shown in Fig. 9 indicates that the introduction of different contaminants led to a decrease in water flux, primarily due to the formation of an emulsion-like contaminant layer on the membrane surface. Nonionic contamination with Tween-20 caused a more significant reduction in water flux compared to SDBS, resulting in a greater flux decrease than that observed with SDBS contamination. Throughout the entire testing period, the desalination conductivity of the PV membrane consistently remained above 99.9 %. Notably, the PEI/SPTA separation layer exhibited exceptional stability against nonionic contamination and demonstrated robust fouling resistance against negatively charged contaminants. Table 5 compares the desalination capacities of inorganic and organic membrane materials, prepared by various research teams under different conditions, to highlight performance differences in diverse experimental setups.

Table 5
An analysis comparing the capacities of different membranes for pervaporation desalination.

Membrane ID	Feed Type	Salt conc. (wt.%)	Temp: (°C)	Flux (kg m^{-2} h^{-1})	Salt Rejection (%)	Ref.
PES/PEI/SPTA	NaCl	3.5	82	180.35	99.97	This work
GO/PVA/PVDF	NaCl	10	65	28	> 99.99	[40]
GO/PAN	NaCl	3.5	90	65.1	~99.8	[41]
GO/PTFE	NaCl	3.5	70	124	>99.99	[42]
Chitosan/GO	NaCl	5	81	30	99.99	[43]
Silica/PVA	NaCl	3.5	22	6.93	99.5	[44]
GO/ceramic	NaCl	3.5	90	48.4	99.7	[45]
GO/PAN	NaCl	3.5	90	65.1	99.8	[41]
GOF/ceramic	NaCl	3.5	90	11.4	99.9	[46]

4. Conclusion

This study successfully employs NIPS technology to fabricate a hydrophilically modified porous PES membrane as the foundational substrate for PV composite membranes. By examining the characteristics of PVA and PEI as separation layer polymers within SPTA and P(AA-AMPS) crosslinking systems, a stable composite layer structure was developed for the first time through solution spraying. Detailed comparative analysis was conducted to evaluate the effects of each system on the structural attributes and performance metrics of PV composite membranes, with particular emphasis on desalination efficiency. The selection of crosslinked structures within the separation layer proved critical for optimizing pervaporation performance. The PES/PEI/SPTA composite membrane consistently demonstrated high salt rejection stability and superior permeation flux under varied conditions of temperature, feed concentration, ionic composition, and contaminants. These findings highlight the advantages of combining a hydrophilic-modified porous PES substrate with a dense hydrophilic PEI separation layer. This approach offers a highly promising avenue for developing advanced pervaporation membranes with robust antifouling capabilities, underscoring its exceptional potential for seawater desalination applications.

CRediT authorship contribution statement

Thi Thi Mar: Writing – review & editing, Writing – original draft, Visualization, Validation, Software, Methodology, Investigation, Formal analysis, Data curation, Conceptualization. **Da Yin:** Data curation, Conceptualization. **Ziyu Fang:** Data curation, Conceptualization. **Tao Wang:** Data curation, Conceptualization. **Xi Dai:** Data curation, Conceptualization. **Bing Cao:** Writing – review & editing, Writing – original draft, Visualization, Validation, Supervision, Resources, Project administration, Methodology, Investigation, Funding acquisition, Formal analysis, Data curation, Conceptualization. **Rui Zhang:** Writing – review & editing, Writing – original draft, Visualization, Validation, Supervision, Resources, Project administration, Methodology, Investigation, Data curation, Conceptualization.

Declaration of competing interest

The authors declare that they have no known competing financial interests or personal relationships that could have appeared to influence the work reported in this paper.

Supplementary materials

Supplementary material associated with this article can be found, in the online version, at doi:10.1016/j.cep.2024.110083.

Data availability

The authors confirm that the data supporting the findings of this study are available within the article [and/or] its supplementary materials.

References

[1] D. Qin, H. Liu, J. Yan, Z. Yu, Z. Du, B. Cao, R. Zhang, Large-scale preparation of UV photo-crosslinked composite membrane with high pervaporation desalination properties and excellent fouling resistance, J. Membr. Sci. 691 (2024) 122175–122184.
[2] Y. Li, E.R. Thomas, M.H. Molina, S. Mann, W.S. Walker, M.L. Lind, F. Perreault, Desalination by membrane pervaporation: a review, Desalination. 547 (2023) 116223–116236.
[3] R. Guo, X. Fang, H. Wu, Z. Jiang, Preparation and pervaporation performance of surface crosslinked PVA/PES composite membrane, J. Membr. Sci. 322 (2008) 32–38.
[4] X. Lu, M. Elimelech, Fabrication of desalination membranes by interfacial polymerization: history, current efforts, and future directions, Chem. Soc. Rev. 50 (2021) 6290–6307.
[5] I. Prihatiningtyas, B. Van der Bruggen, Nanocomposite pervaporation membrane for desalination, Chem. Eng. Res. Design 164 (2020) 147–161.
[6] Y.L. Xue, J. Huang, C.H. Lau, B. Cao, P. Li, Tailoring the molecular structure of crosslinked polymers for pervaporation desalination, Nat. Commun. 11 (2020) 1461–1469.
[7] J. Meng, P. Zhao, B. Cao, C.H. Lau, Y. Xue, R. Zhang, P. Li, Fabricating thin-film composite membranes for pervaporation desalination via photo-crosslinking, Desalination. 512 (2021) 115128–115136.
[8] A.F. Ismail, K.C. Khulbe, T. Matsuura, RO membrane fouling, Rev. Osmosis (2019) 189–220.
[9] R.H. Hailemariam, Y.C. Woo, M.M. Damtie, B.C. Kim, K.D. Park, J.S. Choi, Reverse osmosis membrane fabrication and modification technologies and future trends: a review, Adv. Colloid. Interface Sci. 276 (2020) 102100–102121.
[10] L. Shen, F. Wang, L. Tian, X. Zhang, C. Ding, Y. Wang, High-performance thin-film composite membranes with surface functionalization by organic phosphonic acids, J. Membr. Sci. 563 (2018) 284–297.
[11] N. Shehata, D. Egirani, A.G. Olabi, A. Inayat, M.A. Abdelkareem, K.J. Chae, E. T. Sayed, Membrane-based water and wastewater treatment technologies: issues, current trends, challenges, and role in achieving sustainable development goals, and circular economy, Chemosphere 320 (2023) 137993–138012.

[12] P. Shao, R.Y.M. Huang, Polymeric membrane pervaporation, J. Membr. Sci. 287 (2007) 162–179.
[13] H.Z. Shafi, Z. Khan, R. Yang, K.K. Gleason, Surface modification of reverse osmosis membranes with zwitterionic coating for improved resistance to fouling, Desalination. 362 (2015) 93–103.
[14] R.A. Milescu, C.R. McElroy, T.J. Farmer, P.M. Williams, M.J. Walters, J.H. Clark, Fabrication of PES/PVP water filtration membranes using cyrene®, a safer bio-based polar aprotic solvent, Adv. Polymer Techn. 2019 (2019) 1–15.
[15] Q. Wang, N. Li, B. Bolto, M. Hoang, Z. Xie, Desalination by pervaporation: a review, Desalination. 387 (2016) 46–60.
[16] Y. Wu, J. Zeng, Y. Zeng, H. Zhou, G. Liu, J. Jian, J. Ding, Polyethersulfone-polyvinylpyrrolidone composite membranes: effects of polyvinylpyrrolidone content and polydopamine coating on membrane morphology, structure and performances, Chin. J. Chem. Eng. 38 (2021) 84–97.
[17] G. Wu, S. Gan, L. Cui, Y. Xu, Preparation and characterization of PES/TiO2 composite membranes, Appl. Surf. Sci. 254 (2008) 7080–7086.
[18] N. Widjojo, T.S. Chung, M. Weber, C. Maletzko, V. Warzelhan, A sulfonated polyphenylenesulfone (sPPSU) as the supporting substrate in thin film composite (TFC) membranes with enhanced performance for forward osmosis (FO), Chem. Eng. J. 220 (2013) 15–23.
[19] A. Abdel-Karim, A. El-Kalliny, S. Leaper, P. Gorgojo, M. Badawy, T. Gad-Allah, A review on modified polyethersulfone-based membranes prepared by blending method for water treatment, Egypt. J. Chem. 65 (2022) 677–693.
[20] A. Abdel-Karim, S. Leaper, M. Alberto, A. Vijayaraghavan, X. Fan, S.M. Holmes, E. R. Souaya, M.I. Badawy, P. Gorgojo, High flux and fouling resistant flat sheet polyethersulfone membranes incorporated with graphene oxide for ultrafiltration applications, Chem. Eng. J. 334 (2018) 789–799.
[21] L. Shen, X. Bian, X. Lu, L. Shi, Z. Liu, L. Chen, Z. Hou, K. Fan, Preparation and characterization of ZnO/polyethersulfone (PES) hybrid membranes, Desalination. 293 (2012) 21–29.
[22] D. Qin, H. Liu, T. Xiong, J. Wang, R. Zhang, B. Cao, P. Li, Enhancing the property of composite pervaporation desalination membrane by fabricating a less resistance substrate with porous but skinless surface structure, Desalination. 525 (2022) 115496–115505.
[23] S. Acarer, Effect of different solvents, pore-forming agent and solubility parameter differences on the properties of PES ultrafiltration membrane, Sakarya Univ. J. Sci. 26 (2022) 1196–1208.
[24] S.A. Al Malek, M.N. Abu Seman, D. Johnson, N. Hilal, Formation and characterization of polyethersulfone membranes using different concentrations of polyvinylpyrrolidone, Desalination. 288 (2012) 31–39.
[25] J. Yan, Z. Du, Z. Yu, B. Cao, T. Mar, D. Qin, R. Zhang, Optimization of mass transfer-enhanced chlorine-resistant crosslinked PVA composite membranes for pervaporation desalination desalination 586 (2024) 11872–11882.
[26] T. Mar, Y. Xue, Y. Chang, Z. Yu, Z. Du, B. Cao, R. Zhang, Fabrication and performance optimization of an advanced pervaporation desalination membrane: a study utilizing PVDF and hydrophilic active layer as composite, Results. Eng. 23 (2024) 102760–102772.
[27] J. Wang, B. Cao, R. Zhang, P. Li, Spray-coated tough thin film composite membrane for pervaporation desalination, Chem. Eng. Res. Design 179 (2022) 493–501.
[28] H.S. Mansur, C.M. Sadahira, A.N. Souza, A.A.P. Mansur, FTIR spectroscopy characterization of poly (vinyl alcohol) hydrogel with different hydrolysis degree and chemically crosslinked with glutaraldehyde, Mater. Sci. Eng. 28 (2008) 539–548.
[29] P. Zhao, Y. Xue, R. Zhang, B. Cao, P. Li, Fabrication of pervaporation desalination membranes with excellent chemical resistance for chemical washing, J. Membr. Sci. 611 (2020) 118367–118376.
[30] G. Bai, Y. Han, P. Du, Z. Fei, X. Chen, Z. Zhang, J. Tang, M. Cui, Q. Liu, X. Qiao, Polyethylenimine (PEI)-impregnated resin adsorbent with high efficiency and capacity for CO2 capture from flue gas, New J. Chem. 43 (2019) 18345–18354.
[31] E. Halakoo, X. Feng, Layer-by-layer assembly of polyethyleneimine/graphene oxide membranes for desalination of high-salinity water via pervaporation, Sep. Purif. Technol. 234 (2020) 116077–116088.
[32] H. Zeng, S. Liu, J. Wang, Y. Li, L. Zhu, M. Xu, C. Wang, Hydrophilic SPEEK/PES composite membrane for pervaporation desalination, Sep. Purif. Technol. 250 (2020) 117265–117290.
[33] M. Mohsin, A. Hossin, Y. Haik, Thermal and mechanical properties of poly(vinyl alcohol) plasticized with glycerol, J. Appl. Polym. Sci. 122 (2011) 3102–3109.
[34] A. Kapourani, K. Chachlioutaki, E.G. Andriotis, D.G. Fatouros, P. Barmpalexis, Evaluating PAA/PVA thermal crosslinking process during the preparation of in-situ high-drug loading amorphous solid dispersions, J. Drug Deliv. Sci. Technol. 79 (2023) 104030–104040.
[35] H. Kaur, V.K. Bulasara, R.K. Gupta, Influence of pH and temperature of dip-coating solution on the properties of cellulose acetate-ceramic composite membrane for ultrafiltration, Carbohydr. Polym. 195 (2018) 613–621.
[36] S. Bonyadi, T.S. Chung, Flux enhancement in membrane distillation by fabrication of dual layer hydrophilic–hydrophobic hollow fiber membranes, J. Membr. Sci. 306 (2007) 134–146.
[37] F.U. Nigiz, Preparation of high-performance graphene nanoplate incorporated polyether block amide membrane and application for seawater desalination, Desalination. 433 (2018) 164–171.
[38] Y.M. Xu, Y.P. Tang, T.S. Chung, M. Weber, C. Maletzko, Polyarylether membranes for dehydration of ethanol and methanol via pervaporation, Sep. Purif. Technol. 193 (2018) 165–174.
[39] P.S. Goh, W.J. Lau, M.H.D. Othman, A.F. Ismail, Membrane fouling in desalination and its mitigation strategies, Desalination. 425 (2018) 130–155.
[40] L. Li, J. Hou, Y. Ye, J. Mansouri, Y. Zhang, V. Chen, Suppressing salt transport through composite pervaporation membranes for brine desalination, Appl. Sci. 7 (2017) 856–874.
[41] W.Z. Bin Liang, Genggeng. Qi, Sensen Lin, Qian Nan, Yuxuan Liu, Bing Cao, Kai Pan, High performance graphene oxide/polyacrylonitrile composite pervaporation membranes for desalination applications, J. Mater. Chem. A 9 (2015) 1–9.
[42] R.L. Yimeng Song, Fusheng Pan, Ze He, Hao Yang, Ying Li, ab Leixin Yang, Meidi Wang, Hongjian Wang, Zhongyi Jiang, Ultrapermeable graphene oxide membranes with tunable interlayer distance via vein-like supramolecular dendrimers, J. Mater. Chem. A 7 (2019) 18642–18652.
[43] N. Xiaowei Qian, Qinzhuo Wang, Songcan Ji, Chitosan/graphene oxide mixed matrix membrane with enhanced water permeability for high-salinity water desalination by pervaporation, Desalination. 438 (2018) 83–96.
[44] Z. Xie, M. Hoang, T. Duong, D. Ng, B. Dao, S. Gray, Sol–gel derived poly(vinyl alcohol)/maleic acid/silica hybrid membrane for desalination by pervaporation, J. Membr. Sci. 383 (2011) 96–103.
[45] K. Xu, B. Feng, C. Zhou, A. Huang, Synthesis of highly stable graphene oxide membranes on polydopamine functionalized supports for seawater desalination, Chem. Eng. Sci. 146 (2016) 159–165.
[46] B. Feng, K. Xu, A. Huang, Covalent synthesis of three-dimensional graphene oxide framework (GOF) membrane for seawater desalination, Desalination. 394 (2016) 123–130.